Hybrid Photovoltaic-Thermoelectric System Using a Novel Spectral Splitting Solar Concentrator

Mohammad Alnajideen [a,b] and Gao Min [a, *]

[a] School of Engineering, Cardiff University, Cardiff CF24 3AA, United Kingdom

[b] Faculty of Engineering, Mutah University, Al-Karak 61710, Jordan

Abstract

A hybrid photovoltaic-thermoelectric (PV-TE) system employing a novel solar concentrator is designed and constructed to demonstrate the feasibility of improving the overall efficiency of light-to-electricity conversion based on spectral splitting strategy. The concentrator consists of four rectangular dichroic mirrors arranged in a crossed V-trough configuration that reflects and concentrates the visible spectrum onto a photovoltaic cell in the centre while passes the infrared spectrum onto a thermal absorber to produce heat for a thermoelectric generator. The experimental results show that the overall efficiency of the hybrid PV-TE system is 16.9% compared to 15.9% of the same configuration except for using specular aluminium mirrors. An increase in the overall efficiency by 6.3% was achieved due to thermoelectric harvesting of the light energy in infrared spectrum. The results also show that a significant increase in the power output from 12.41 mW in the bare cell to 62.04 mW of the same cell in the concentrated system, indicating the advantages of using concentration system, particularly beneficial to high-cost solar cells, such as GaAs and GaInP.

***Keywords**: Spectral splitting; photovoltaic; thermoelectric; dichroic mirror; solar concentrator*

Nomenclature

λ_c	Cut-off wavelength	PV	Photovoltaic
AL	Aluminium mirror	P-V	Power – voltage (curve)
DM	Dichroic mirror	R	Resistance
I-S	Impedance spectroscopy (curve)	TE	Thermoelectric
I_{sc}	Short-circuit current	V_{oc}	Open-circuit voltage
I-V	Current- voltage (curve)	VSC	V-trough Solar Concentrator
OVSC	Onagraceae V-trough Solar Concentrator	ZT	Figure-of-merit
P_{max}	Maximum power output	ΔT	Temperature difference

1. Introduction

Solar energy can be harvested using numerous types of technologies, the most popular types are solar thermal collectors (STC) and photovoltaics (PV) [1]. Solar thermoelectrics (STE) are one of the possible technologies that are currently under investigations [2, 3]. The main challenge facing those technologies is to convert solar radiation efficiently and cost-effectively. STCs and STEs convert less than 25% and 5%, respectively, of sunlight to electricity [2, 4], whereas commercial PV cells can convert about 10-25% (or 10-47% for laboratory cells) of sunlight to electricity [1, 5]. It is possible to combine PVs with thermal or TE generators as hybrid energy systems to increase the conversion efficiency of sunlight [3]. Additional benefits from hybrid PV-TE systems can be achieved by using solar energy concentrators, aiming to increase the power output and reduce the materials cost [2, 5].

There are several factors that degrade the efficiency of solar energy conversion including optical, thermal, mechanical and electrical losses [6]. A major factor for energy loss in PV cells is the spectral mismatch between the solar spectrum and the PV bandgap energy [7], which often turns into heat [8, 9]. Therefore, integrating them with thermal receivers is a possible solution to extract heat generated by PVs to be converted into useful energy [10, 11]. In conventional tandem PV-TE systems, the sunlight strikes the PV cells, which partially converts into electricity and partially into heat [12]. The heat can be collected by a TE generator underneath the PV cell and convert it into electrical power [13]. However, the thermal coupling between the PV and TE is a big challenge. Using a TE with longer legs will lead to an increase in the PV temperature but using shorter legs will reduce the temperature difference across the TE generator and hence the power output from the TE [3, 12]. In addition, the geometry of the TE generator is a trade-off between the materials consumption and the conversion efficiency [14, 15].

Spectral splitting is a promising approach for efficient utilization of sunlight. The basic principle of spectral splitting is to divide the solar spectrum into two or more spectral bands and allocate each band to the most efficient energy convertor. This approach has the potential to address the issues of spectral mismatch in PV cells [16, 17] and thermal coupling between PV and TE in conventional tandem systems [18, 19]. In addition, it can mitigate the temperature increase in PV cells, especially when using solar concentration, and consequently improve the PV lifetime [20, 21]. Spectral splitting can be achieved by using various types of optical [22-24] and fluid-based filters [25-27]. An efficient and readily available approach is to employ commercial interference optical filters known as the dichroic mirrors (DMs) [28-30]. The DMs are made from non-absorbing materials, which have high-optical performance and suitable for a wide range of PV technologies and PV-T hybrid configurations [31-33]. Commercial DMs are only available in flat architecture with two angles of incidence (0˚ and 45˚) [34-36] and their cost depends on the complexity of production, optical and material specifications [37-39]. The DMs have been employed to increase the conversion efficiency of PV systems using single or tandem structures [40-42]. Light concentration has also been proposed to fit in front or behind spectral splitting for further improvement [43, 44].

It has been reported that the applicability of DMs for solar energy conversion is questionable [28, 45]. To date, there is no successful demonstration of simultaneous beamsplitting and light concentration using flat-surface DMs and there are no experimental studies on the performance of such hybrid PV-TE system based on spectral splitting [19-50]. In addition, the use of commercial flat mirrors makes it impossible for direct adoption of the configuration of crossed compound parabolic concentrators (CCPC) [31, 51, 52]. Consequently, the structure of a modified V-trough solar concentrator (VSC) is employed, which is referred to as the “Onagraceae VSC” (OVSC) because its double-trough configuration looks like Onagraceae flowers [53]. In this work, we report a novel PV-TE hybrid system based on dichroic-mirror OVSC to concentrate the visible light to a PV cell and infrared radiation to a TE generator. Experimental investigations were carried out to evaluate the performance of this hybrid PV-TE system.

2. System Description and Experimental Setup

Fig. 1 shows schematic diagram of the novel hybrid PV-TE system. The structure of the concentrator is the same as the OVSC described in [53], except that the aluminium (AL) mirrors are replaced with dichroic mirrors (DM), which enables light splitting. By using such a DM concentrator, the sunlight in the visible spectrum will be directed to a PV cell by reflection and the infrared spectrum will pass through and fall on a thermal absorber that converts light into heat for a TE module, enabling efficient utilization of solar energy over its full spectrum.

Compared to a conventional concentrator PV system using AL mirrors, the key advantage of the hybrid system is that the infrared radiation that has no use for the PV cell is now separated and utilized by the TE module, resulting in an improvement in system efficiency. The performance of the proposed hybrid PV-TE system depends on i) the spectral performance of the DM, ii) the effectiveness of the concentrator design, iii) the conversion efficiency of the PV cell and TE module, and iv) appropriate system integration.

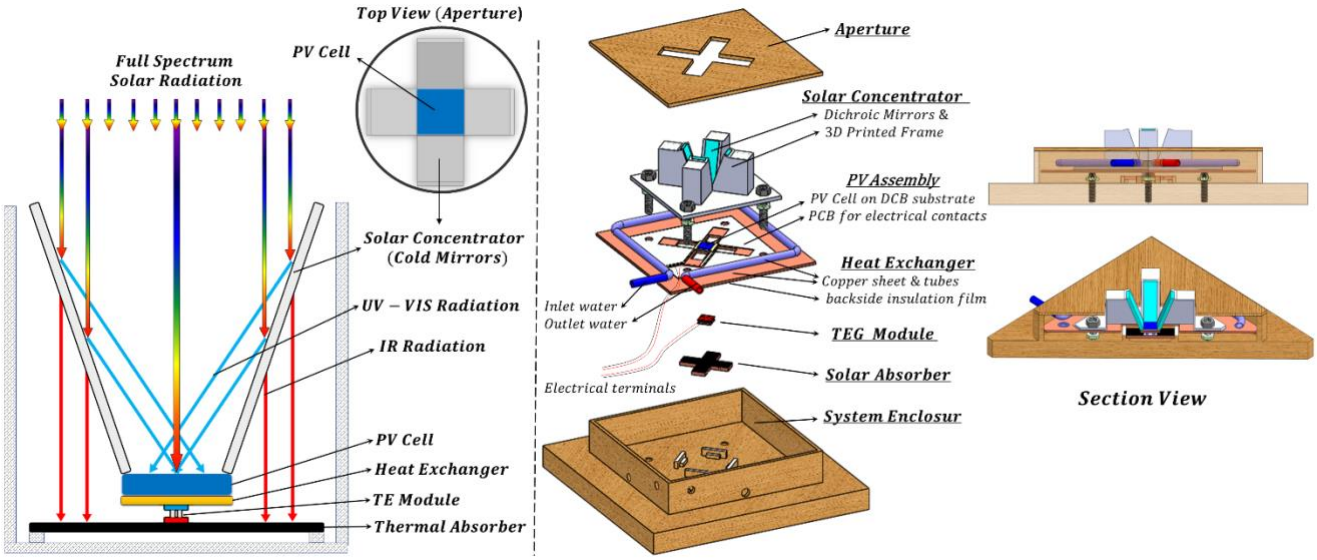

Fig. 1: The schematic diagram of the novel hybrid PV-TE system.

Following the conceptual design shown in Fig. 1, a prototype hybrid PV-TE system was constructed. Fig. 2 shows photographs of the constructed prototype and experimental setup. The angle of the dichroic mirrors in the OVSC concentrator is 71˚, which was selected based on a trade-off between higher concentration ratio and minimum optical loss described in [53]. Four dichroic mirrors of 32 mm x 10 mm were cut from a large sheet of 101 mm x 127 mm [54], cleaned using the IPA solution in an ultrasonic bath and glued onto a 3D-printed frame as shown in Fig. 2b-1. This concentrator is referred to as the dichroic concentrator, “DM-OVSC-71”.

A single-junction GaInP PV cell [55] was used to achieve the best spectrum match with the chosen dichroic mirror, as discussed in section 3.2. The PV cell (10 mm x 10 mm) was mounted on a direct-copper-bonded (DCB) alumina substrate [56]. The DCB alumina substrate has excellent electrical insulation and thermal conductivity (24-28 W/m.K). A printed-circuit-board (PCB) was designed and fabricated to ensure secured electrical connection to the PV cell, which is located on the top of the heat exchanger. Fig. 2b-2 shows the photograph of the fabricated PV cell assembly. It is worth mentioning that the small solar cells were used in this design due to their availability (particularly, GaAs and GaInP cells) and the limitation of solar simulator area (60 mm x 60 mm) available for the tests. However, we believe that there are no fundamental barriers to scale-up of the system that can accommodate the large size (e.g., 150mm x 150mm) solar cell, which could cause degradation in the performance.

A thermal absorber was placed at the bottom to collect the infrared radiation that passes through the dichroic mirrors. The absorber was made from a copper plate in a cross shape using a CNC machine. The top surface of the plate was cleaned using IPA solution and painted with a black high-temperature PNM paint [57] to improve light absorption, except for the central area (10 mm x 10 mm), where a TE is mounted on the top of it. The cross plate consists of five equal squares (four painted and one unpainted) and five tiny holes were made by drilling from the sides of the cross plate (i.e., absorber) to reach the centre of each square. Five K-type thermocouples [58] were inserted inside the holes for monitoring the temperature distribution of the plate. The

edge of the plate (i.e., thermal absorber) was rested on the wooden supports inside the wooden box with a gap of 6 mm between the absorber back-surface and the inner surface of the box to minimize conductive heat loss from the thermal absorber. The absorber was surrounded by wooden fingers to prevent it from potential slide. A TE module was sandwiched between the thermal absorber and a heat exchanger, which is shared with the PV cell. The hot side of the TE module was positioned on the top of the central area of the absorber (Fig. 2b-4) and the cold side was in contact with the shared heat exchanger. All gaps between interfaces were filled with the heat sink compound [59] to ensure good heat transfer across the interfaces.

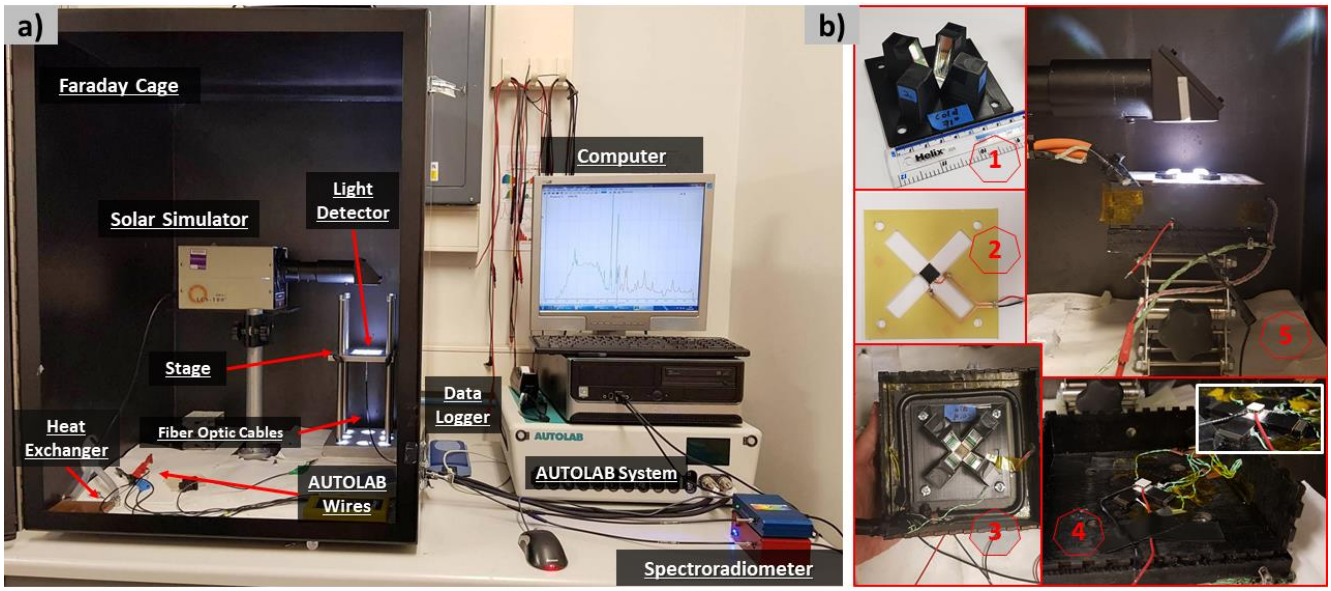

Fig. 2: The photograph of the a) characterization system and b) the experimental novel hybrid PV-TE system, 1) dichroic concentrator, 2) the PV cell assembly, 3) the assembly of the dichroic concentrator, PV and heat exchanger, 4) TE mounted onto a thermal absorber and 5) the full assembly of the hybrid PV-TE system.

The water-cooled heat exchanger can be seen in Fig. 2b-3, which consists of a copper plate and tube assembly. It removes the heat from the PV and TE, which are in contact with a copper plate on the top and from the bottom, respectively, and dissipate it into the water. The copper plate was cut into a square shape with four rectangle holes arranged around the central part. The rectangle holes allow the infrared light to pass through and reach the thermal absorber. The uncut central area of 10 mm x 10 mm is for mounting the PV and TE. A copper tube was configured to a square shape and was soldered on the top of the copper plate, close to its edges. The inlet and outlet of the copper tube were connected to a silicon tube with the inlet connected to tap-water and the outlet left open to drain in a sink. Two channels were made on the heat exchanger close to the centre to accommodate K-type thermocouples for measuring the temperatures of the PV and TE on its cold side. In addition, two thermocouples were placed inside the copper tube at the inlet and outlet, respectively for measuring the water temperatures. All gaps were filled with heat sink compound [59]. The bottom surface of the heat exchanger was insulated using a Kapton film (except the uncut central area for mounting a TE) to minimize the heat convection between the heat exchanger and the thermal absorber. A thermocouple was placed inside the Faraday cage (close to the testing area) to measure the temperature inside the box and the ambient.

The whole setup is mounted inside a wooden box, which was made of birch plywood to provide good thermal insulation. The apertures for incident light were cut using the laser machine and the inner and outer surfaces of the box were painted black. The dimension of the overall system is approximately 140 mm x 140 mm x 40 mm). A similar concentrator using high-reflective thin-film aluminum (AL) mirrors [60] instead of the dichroic mirrors (DM) was also fabricated for comparative study, which is referred to as AL-OVSC-71.

The performance of the PV cells, TE modules, thermal absorber, aluminum concentrator and the hybrid PV-TE system were characterized using the testing setup illustrated in Fig. 2a. The key facilities of the testing setup are i) a class ABB solar simulator [61] as the light source, ii) an AUTOLAB Instrument [62] for Current-Voltage (I-V) and Impedance Spectroscopy (I-S) measurements, iii) a Spectroradiometer [63] for light spectrum determination, iv) a Pyranometer [64] for light intensity measurement, v) a computer for data acquisition and control. The solar simulator and the test assembly were placed securely inside a Faraday cage to prevent any external light/electromagnetic interferences. The measurements were carried out under the standard testing condition of one sun irradiance (1000W/m^2), AM1.5G and 25˚C.

3. Results and Discussion

3.1. Optical Performance of Dichroic Mirror

The reflection and transmission coefficients of the dichroic mirror used in this work were measured as a function of wavelength for different angle-of-incidence (AOI) from 0˚ to 85˚ in a step of 5˚ to study the influence of the AOI on the performance of the mirror. The results are shown in Fig. 3, providing useful information for the design of the optical component of the system. For clarity, Fig. 3 only shows the data of three representative AOIs and the data for other AOIs are available in Appendix-A (Fig. A-1). Fig. 3a also includes the reflection coefficient of the aluminium mirror (AL) [60] for corresponding AOIs.

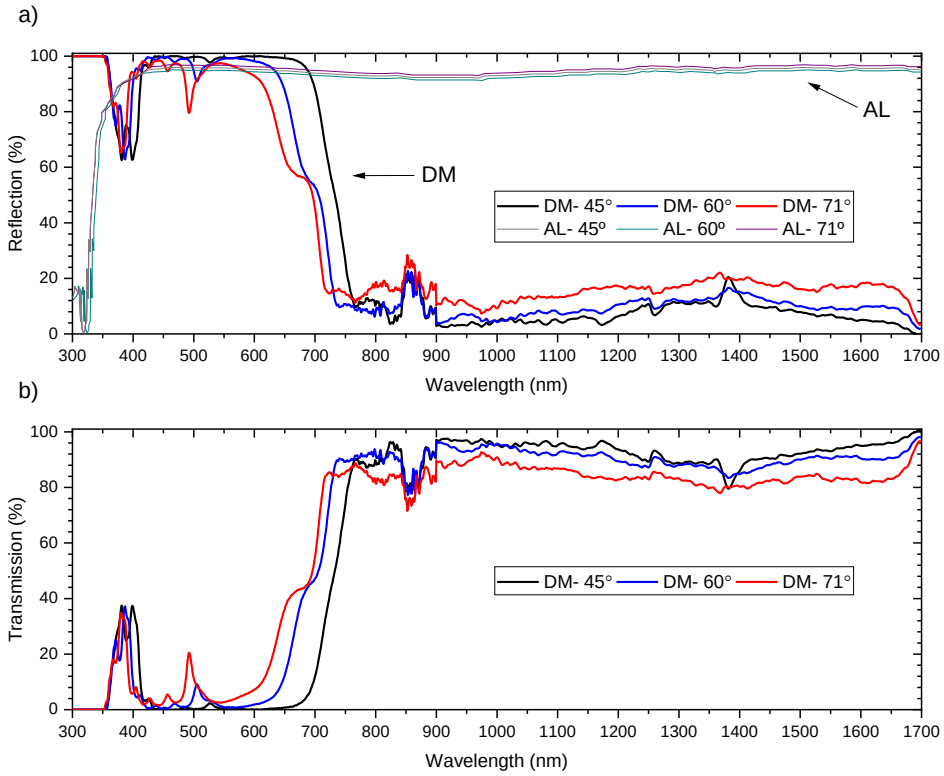

Fig. 3: The spectral response of the dichroic mirrors employed for this study for different angle-of-incidence. a) the reflectance of the dichroic mirror (DM) and aluminum mirror (AL), and b) the transmittance of DM and AL.

It can be seen that the AL mirror shows high reflection for all measured AOIs and wavelengths, except for the UV range. The dichroic mirror shows high reflection over the UV-VIS range and high transmission over the IR range with the cut-off wavelength, λ_c, at 740nm, 712nm and 700nm for AOIs of 45˚, 60˚ and 71˚, respectively. This result indicates that the optical performance of the dichroic mirror is sensitive to the AOI, which raises a challenge in the design for practical operation, where the angle of the incident sunlight changes with time. In this work, only

the ideal operating condition was investigated (i.e., the incident light is perpendicular to the aperture surface of the concentrator). In the design, the concentrator angle of 60˚ and 71˚ were selected because the tilt angle of the mirror in the proposed solar concentrator must be in the range of 60°-75° as required by OVSC design, whereas 45˚ is a reference angle of the commercial dichroic mirror. The spectral range reflected by the dichroic mirror represents the PV-band for solar cells while the spectral range transmitted through the dichroic mirror represents the TE-band for thermoelectric generators.

3.2. PV Cell Characterization

The PV cells were illuminated using a solar simulator under one sun (full spectrum) to characterize their electrical performance as the reference for studying their performance when illuminated under the partial spectrum. The I-V curves of the cells were acquired using the AUTOLAB before and after spectral splitting using the dichroic mirror at the standard angle-of-incidence of 45˚ and the angles of 60˚ and 71˚, which are the angles used in the OVSC concentrators. Fig. 4 presents the I-V curves of the Si, GaAs and GaInP cells measured under the full spectrum and partial spectrum. The photocurrent, voltage and power output of the solar cells are decreased under the partial spectrum using a dichroic mirror (compared to the values obtained under the full spectrum of the same light intensity). The level of reduction varies depending on the type of the PV cells and the angle-of-incidence of the mirror.

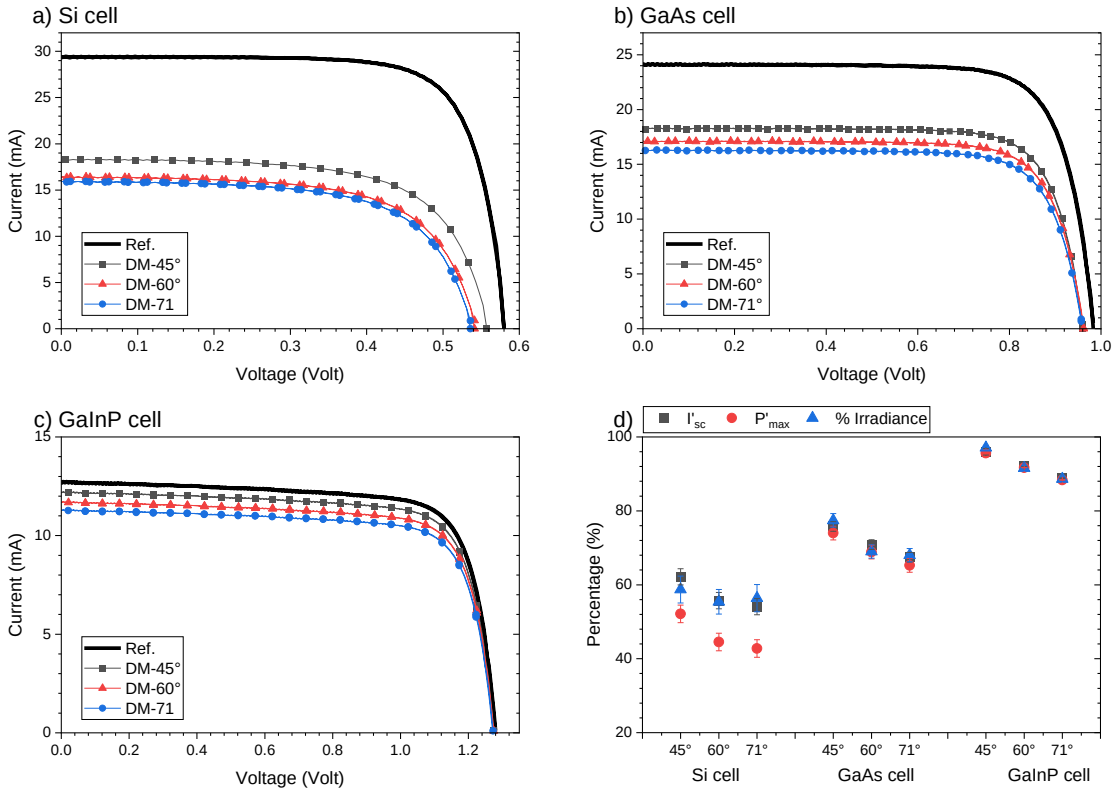

Fig. 4: I-V curves obtained under full spectrum illumination (Ref) and partial spectrum illumination (DM) for three different angle-of-incidences. a) Si cell, b) GaAs cell, and c) GaInP cell; and d) the ratio of the I_{sc} and P_{max} of the PV cells under partial spectrum illumination to that under full spectrum and the ratio of the actual light intensity reflected onto the PV cells to the expected light intensity available over their respective wavelength ranges for Si, GaAs and GaInP cells.

It can be seen that the short-circuit current (I_{sc}) decreased significantly while the open-circuit voltage (V_{oc}) is reduced slightly when the PV cells were illuminated by the partial spectrum of the reflected light, compared to full spectrum illumination without the mirror. This is because the I_{sc} is dependent on the light intensity linearly, whereas the V_{oc} is dependent on the light intensity logarithmically. The reduction in I_{sc} can be explained based on the spectral response of the mirror shown in Fig. 3a and the measured EQE data of the PV cells shown in Fig. A-

2 (Appendix) The Si cell responds to the spectral range of 300nm – 1200nm, but the spectral energy reflected onto the Si cell by this mirror only covers a wavelength range from 300nm to 740nm for the case of AOI at 45˚. Considering an average reflectance of approximately 95% of the mirror, this represents more than 40% reduction in the light intensity illuminated on the Si cell, leading to a decrease of 38% in I_{sc}. For the cases of AOI at 60˚ and 71˚, the corresponding reduction in I_{sc} are 44% and 46%, respectively. The maximum power output, P_{max}, exhibits a further 10% reduction due to a noticeable decrease in the V_{oc} of the Si cell after spectral splitting.

The GaAs cell has a response range between 300nm and 900nm. However, the cut-off wavelength of the mirror is around 700nm. As a result, the light over the range of 700nm – 900nm will pass through the mirror, instead of being reflected on the GaAs cell. This leads to a reduction in I_{sc} by 24%, 29% and 33% for the AOI at 45˚, 60˚ and 71˚, respectively. The corresponding reduction in P_{max} is 27%, 31% and 35%, respectively. The level of reduction in P_{max} of the GaAs cell is smaller than that of the Si cell because the spectral mismatch in the GaAs cell is less severe than that of the Si cell.

The I_{sc} and P_{max} of the GaInP cell obtained under the partial spectrum are very close to these obtained under the full spectrum. This is because the dichroic mirror used in this study offers good spectral match to the GaInP cell. Compared to the full spectrum data, I_{sc} of the GaInP cell decreased by only 4%, 8% and 11% for the AOI at 45˚, 60˚ and 71˚, respectively. The reduction in P_{max} is almost the same as that in I_{sc} due to a negligible reduction in the V_{oc} of the cell. Fig. 4d illustrates the correlation between the spectral characteristics of the dichroic mirror and the electrical performances of the PV cells under the full and partial spectrum irradiances. Among the three types of PV cells tested, the GaInP cell offers the best match to the dichroic mirror employed in this study. The results confirm that the solar energy outside the matched spectrum of the PV cells does not contribute to electricity generation. Clearly, in the case of GaInP cells, the energy over the wavelength range of 700nm - 2500nm can be exploited for other utilizations, such as producing heat.

3.3. TE Geometry Optimization

3.3.1. Determination of Thermal Input

Using the system described in section 2, the light with wavelength of >700nm will pass through the dichroic mirror to reach the thermal absorber, which converts the light into heat to drive a TE module. In order to select the most suitable TE module, an experimental investigation was performed to determine the amount of thermal energy absorbed by the absorber. The temperature of the thermal absorber was measured continuously during heating-up when the absorber was exposed to the light (Appendix-A, Fig. A-3). In this experiment, the thermal absorber was isolated, i.e., disconnected from the TE module and heat exchanger. After reaching the steady state, the average temperature of the five locations distributed over the thermal absorber was found 73.2˚C and 57.8˚C for one-sun illumination without and with the dichroic mirror, respectively. The uniformity of temperature across the absorber is 96.8%. The amount of heat absorbed by the thermal absorber can be calculated using the slope technique [65] at an initial heating-up period (the first 10 seconds in this study). The rate of heat absorption was found to be 398mW and 218mW corresponding to the full and partial spectrum illumination, respectively. The results indicate that only 45% of solar energy is allocated to the GaInP cell while 55% of solar energy to thermoelectric generator.

The incident light power was also measured using the pyranometer and the spectroradiometer. The results were found 400mW and 220mW, respectively, which indicates the absorber efficiency is approximately 98%. The slope technique is only valid when the heat loss is negotiable, i.e., in the case of a very small temperature

difference between the absorber and the ambient. When the temperature of the thermal absorber increases, the heat loss becomes significant. The heat retained by the thermal absorber decreases with increasing the temperature of the absorber due to increased heat loss. This decrease will continue until reaching a steady-state value, where the heat absorbed is equal to the heat lost.

3.3.2. Characterization of TE Modules

Selection of appropriate TE module is crucial to achieve the maximum power output from the given thermal input. Six commercial TE modules of varied sizes [66] were investigated experimentally in order to identify the most suitable module for integration into the hybrid PV-TE system. Since the central area of the thermal absorber in the hybrid system is 10mm x 10mm, a convenient size of the TE module for integration should be equal or smaller than 10mm x 10mm. The geometrical parameters of the TE modules investigated are listed in Table 1. The theoretical outline for calculating the power output and conversion efficiency of the TE modules can be found in refs [67-69].

Table 1: Geometrical parameters of the TE modules (L, W and H are the length, width and height of the modules. N is the number of thermocouples, l_{TE} is the length of the TE element, A_c is the cross-sectional area of a single TE element and A_{TE} is the total cross-sectional area of all TE elements in a module).

TE	Dimensions L (mm) x W (mm) x H (mm)	N	A_c (mm^2)	l_{TE} (mm)	A_{TE} (mm^2)	(A_{TE}/l_{TE}) (mm)
M-I	6.00 x 4.00 x 3.00	11	0.25	1.50	5.50	3.67
M-II	8.00 x 8.00 x 3.80	7	1.00	1.50	14.00	9.33
M-III	4.00 x 4.00 x 3.00	7	0.25	1.50	3.50	2.33
M-IV	6.00 x 6.00 x 3.80	7	0.64	1.50	8.96	5.97
M-V	4.00 x 4.00 x 2.70	7	0.36	1.10	5.04	4.58
M-VI	10.00 x 10.00 x 3.20	17	1.00	1.60	34.00	21.25

Each TE module was integrated into the concentrator system as shown in Fig. 1 and evaluated under the full spectrum (without the dichroic mirror) and the partial spectrum (using the dichroic concentrator DM-OVSC-71). The I-V, P-V and P-R curves of the modules are presented in Fig. 5. The temperatures measured across the TE modules after the steady state was reached are listed in Table 2. It can be seen from Fig. 5 that the voltage, current and power outputs were reduced on average by 40%, 40% and 65%, respectively when the light intensity was changed from full spectrum to partial spectrum. It can also be seen that the power output of the TE modules varies significantly with the size. The power output of module VI is about 5 times as big as module III, demonstrating the importance of selecting the appropriate module for the specific application. The power output appears to increase with increasing the A_{TE}, with the largest power output being obtained in module VI. This trend is true for both cases under full-spectrum and partial spectrum irradiance.

Table 2: The steady state temperatures difference (ΔT) between the hot and cold side of the TE modules and the temperature difference (ΔT_w) between the inlet and outlet of the cooling water.

TE	T_h ± 0.9 ˚C		T_c ± 0.8 ˚C		ΔT (˚C) ± 1 ˚C		ΔT_w (˚C) ± 0.5 ˚C	
	Full Spectrum	Partial Spectrum	Full Spectrum	Partial Spectrum	Full Spectrum	Partial Spectrum	Full Spectrum	Partial Spectrum
M-I	37.5	27.5	17.1	15.6	20	12	2.1	1.5
M-II	34.8	26.8	18.2	16.3	16	11	2.2	1.6
M-III	36.2	27.1	15.6	15.0	21	12	2.1	2.0
M-IV	35.6	25.8	16.7	14.6	19	11	2.0	1.2
M-V	35.6	27.5	16.7	16.2	19	11	2.2	1.5
M-VI	30.9	25.1	17.3	16.1	14	9	2.2	1.6

Among small modules (I, III, IV and V), module IV generates the largest power output because its A_{TE} is bigger than that of module I, V and III. The power output from module V is smaller than that produced by module

I, not only because its smaller A_{TE} but also a shorter length. Module III has the smallest A_{TE} and generates the lowest power output. Although this trend agrees with the theory, the power reduction in small modules is much more significant due to considerable heat loss occurred in the thermal absorber. For a given heat input, the TE modules with a small A_{TE}/l_{TE} will result in a larger ΔT and higher temperature on the hot side (if the cold side maintained at a fixed temperature). However, the temperature difference obtained from the experiment of this work (Table 2) for small modules are significantly smaller than the calculated values without heat loss, confirming that the heat loss from the thermal absorber is the main factor that is responsible for the significant reduction of the power output in small modules. If the heat loss can be minimized, the power output of small modules can be significantly improved. Since the heat loss from the largest module (Module VI) is much small, the experimental value agrees roughly with theoretical calculation. However, due to the temperature difference across the large module are relatively small, the uncertainty of the temperature data is increased to about 10%. Nevertheless, the reliability and accuracy of the data is still sufficient.

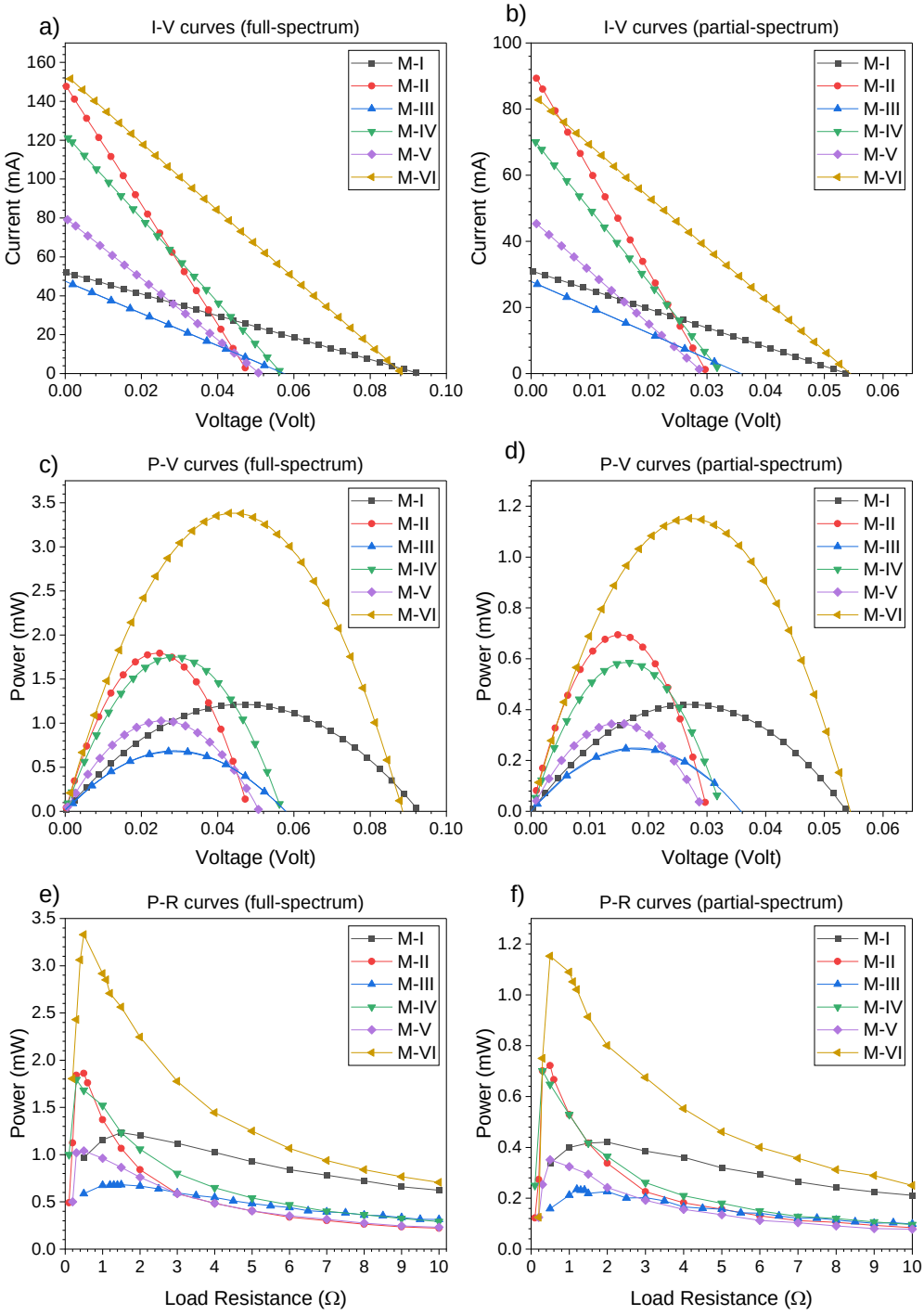

Fig. 5: TE modules testing results. a) I-V curves under full spectrum illumination, b) I-V curves under partial spectrum illumination, c) P-V curves under full spectrum illumination, d) P-V curves under partial spectrum illumination, e) P-R curves under full spectrum illumination, and f) P-V curves under partial spectrum illumination.

It can be seen that the maximum power outputs determined using I-V curves (Fig. 5c andFig. 5d) are in reasonable agreement with these obtained from the matched-load tests (Fig. 5e and Fig. 5f). The Seebeck coefficient of the TE materials (α) can be estimated using the open-circuit voltages and corresponding temperature differences measured across the TE modules. The internal resistances of the TE module (R_{TE}) were determined experimentally using three methods: the I-V curves of Fig. 5, the I-S curves (Appendix-A, Fig. A-4) and the P-R curves corresponding to the matched-load (Fig. 5). The dimensionless figure of merit of the TE modules (ZT) were determined from impedance spectroscopy [70]. The results are shown in Table 3.

Table 3: The material parameters of the TE modules.

TE	α $(\mu V/K)$ ± 1	ZT ± 0.1	I-S curves ± 0.02 Ω	I-V curves ± 0.01 Ω		Matched load Ω ± 0.05 Ω	
			R_{TE} (Ω)	Full Spectrum R_{TE} (Ω)	Partial Spectrum R_{TE} (Ω)	Full Spectrum R_{TE} (Ω)	Partial Spectrum R_{TE} (Ω)
M-I	208	0.7	1.65	1.50	1.61	1.25	1.15
M-II	220	0.7	0.24	0.26	0.27	0.35	0.40
M-III	170	0.6	1.06	1.12	1.28	0.65	0.60
M-IV	200	0.7	0.37	0.40	0.40	0.40	0.35
M-V	175	0.7	0.48	0.50	0.52	0.50	0.50
M-VI	210	0.7	0.56	0.59	0.67	0.60	0.65

In general, the selection of appropriate TE modules is guided by achieving the best performance at minimum cost. In this research, the maximum power output is a priority and can be met by using module VI, which has the largest A_{TE} at a slightly higher cost. It reduces the area between the thermal absorber and the ambient, resulting in less heat loss due to convection and radiation. In addition, a larger area provides a mechanically stable mounting with the thermal absorber and heat exchanger.

3.4. Performance of Prototype Hybrid PV-TE System

3.4.1 Optical Characteristics

Fig. 6 presents the reflection and transmission spectra of the dichroic mirror at 71˚. The reflected spectrum is directed onto the PV cell (blue line) and the transmitted spectrum is shone on the thermal absorber for the TE module (red line). The spectra were measured using a spectroradiometer over the wavelength range of 300nm - 1700 nm, which account for more than 95% of light energy in the whole solar spectrum. The spectral splitting strategy of using the GaInP cell and thermal receiver is also shown in the figure. The blue area represents the ideal spectrum for the GaInP cell and the red area for the thermal absorber. Clearly, the measured spectra for the PV cell and TE module are very close to the design requirement within about 10% difference. It is to be noted that Fig. 6 shows the results of the experiment using a single dichroic mirror (i.e., no concentration).

The same experiment was repeated using the developed concentrator described in Fig. 1 and the results are displayed in Fig. 7, where the DM-OVSC-71˚ represents a concentrator fabricated using the dichroic mirrors as its reflective surfaces and the AL-OVSC-71˚ represents the same concentrator but using the aluminium foils as its reflective surfaces. It can be seen from Fig. 7a that the spectrum obtained using the dichroic concentrator is very similar to that obtained using the aluminium concentrator over the PV-band of the GaInP cell. However, the aluminium concentrator concentrates almost the entire solar spectrum onto the PV area, whereas the dichroic concentrator concentrates only the useful part of the spectrum (300nm - 700nm) onto the PV area while the majority of light beyond 700 nm are transmitted to the thermal absorber as shown by Fig. 7b. Ideally, a dichroic concentrator for the GaInP cell should only reflect the light within 300nm-700nm onto the PV cell area. In practice, the dichroic concentrator still reflects a small portion of the light in the spectrum range of >700 nm onto the PV cell. Nevertheless, it is significantly less than that by the aluminium concentrator. The results in Fig. 7 represent the average irradiances measured across the receiver area (i.e., PV cell, thermal absorber), with a 95% uniformity across the receiver.

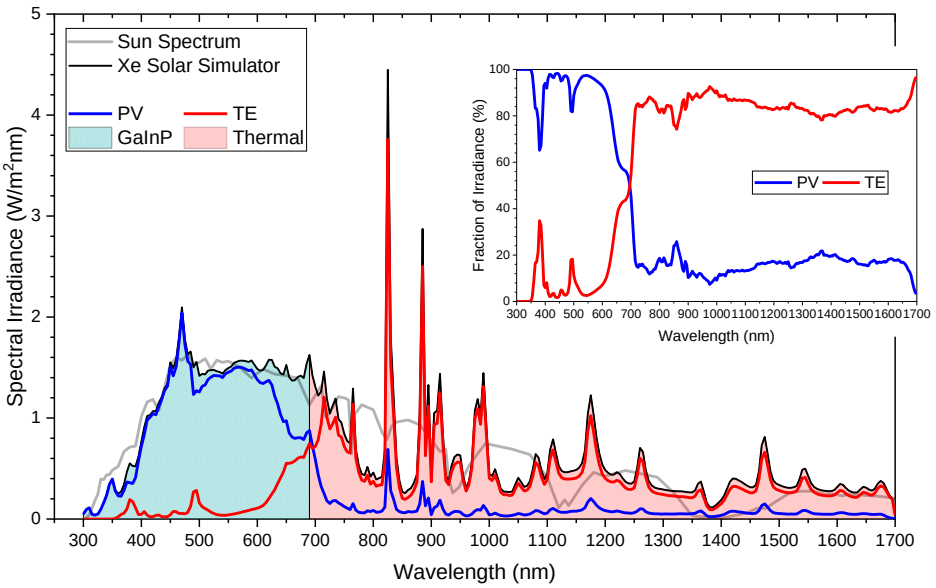

Fig. 6: The measured spectral irradiances of the reflected light (blue) and transmitted light (red) by a dichroic mirror. The inset is measured reflectance and transmittance of the dichroic mirror.

The concentration ratio of concentrators can be determined by direct measurement of light irradiance on the PV area using the spectroradiometer. Since the dichroic mirror only reflects the light over the PV band, the concentration ratio is determined from the total irradiance within the wavelength range of 300nm - 700nm using a concentrator divided by the total irradiance over the same wavelength range without a concentrator. Using the data presented in Fig. 7a, the total irradiances can be calculated by numerical integration of the areas below the measured spectral profiles. The concentration ratio of the concentrators investigated are 4.73x and 4.60x for the aluminium and dichroic concentrators, respectively.

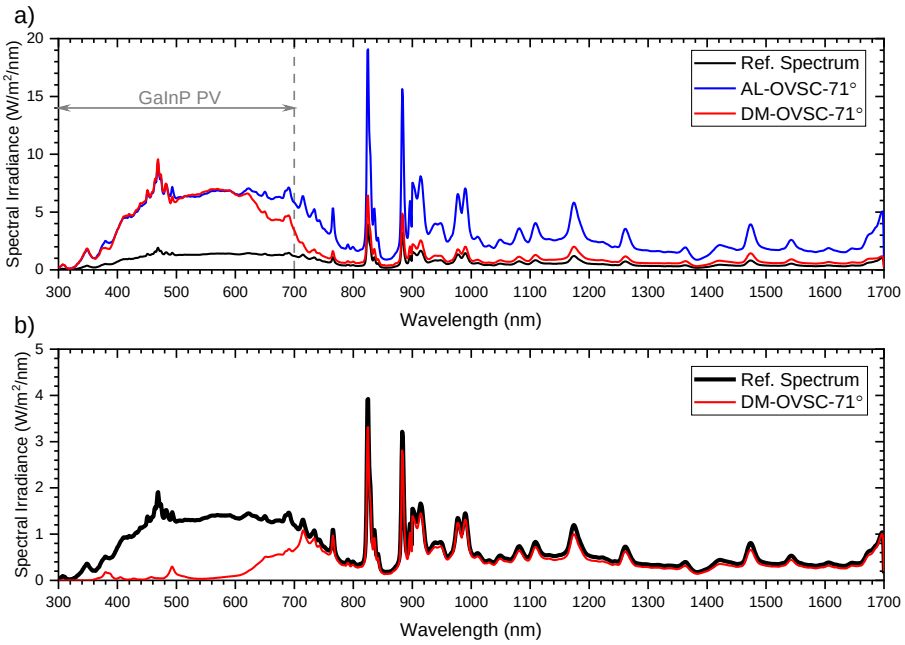

Fig. 7: The spectral irradiances measured using spectroradiometer. a) the reflected spectra by the dichroic and aluminum concentrators (the spectrum of one-sun reference is included for comparison), and b) the transmitted spectrum through the dichroic concentrator.

3.4.2 PV Performance

Fig. 8 presents the I-V and P-V curves of the GaInP cell measured under one sun without concentration and with concentration using the dichroic and aluminium concentrators. The results show that the GaInP cell

produces similar power outputs for both dichroic and aluminium concentrators, with a slightly lower value for the dichroic concentrator (by 2.8%). The I_{sc} and P_{max} of the cell using the dichroic concentrator were 4.60 and 5.00 times of the cell without concentration (bare cell). The PV cell efficiency using both concentrators is almost the same, which is 15.9%. Compared to the efficiency of 14.6% without concentration (i.e., the bare cell), the efficiency of using the concentrators is increased by 8.9%.

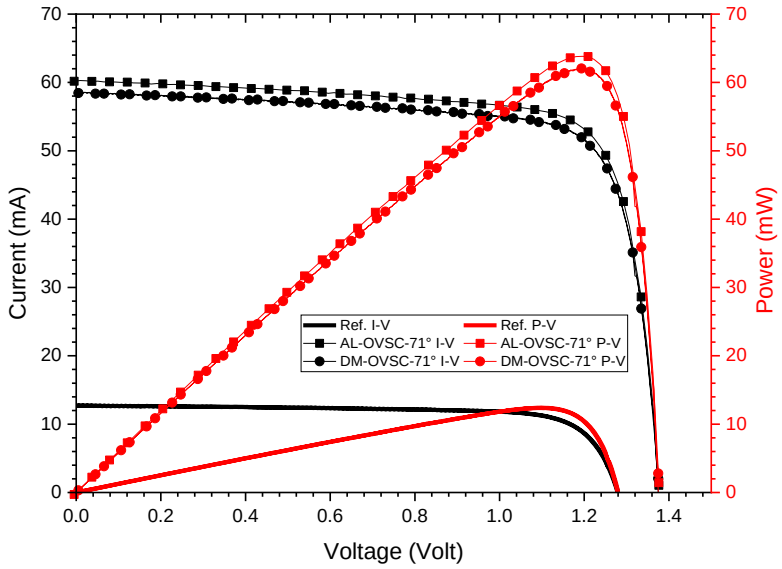

Fig. 8: The I-V and P-V curves of the GaInP cell using the aluminium and dichroic concentrators compared to the bare cell.

The concentration ratio of a concentrator can also be determined from I-V measurement. It is the ratio of the I_{sc} of a PV cell measured using the concentrator to that measured without the concentrator (i.e., bare cell) [53]. The result is the same as that measured using the spectroradiometer, which is 4.60x. The concentration ratio of the aluminium concentrator measured using the PV cell is (4.73x) is slightly lower than that using the spectroradiometer (4.75x). The difference is probably due to the fact that the small gap exists between the PV cell and the aluminium reflectors to avoid electrical fault.

The results above demonstrate that a high-performance dichroic solar concentrator can produce similar performance to conventional specular aluminum concentrators for the GaInP cells. It is to be noted the reflectivity of the thin-film aluminium reflectors employed in this study is already very high (95%) [60]. This indicates that the dichroic concentrator is likely to be better than commercially available concentrators that use the most common reflective materials that have an average reflectivity of 80%-90% [71-75]. It is worth mentioning that the dichroic mirror at an angle of 71˚ is selected rather than 60 ˚ for this study because the geometrical concentration ratio of the OVSC at this angle is 5.12x, whereas it is 3.00x for the concentrator with a tilt angle of 60 ˚. This means a higher solar concentration ratio can be obtained at a larger title angle. More details are available in ref [53].

3.4.3 Overall Performance of the Hybrid PV-TE System

The prototype hybrid PV-TE system that consists of a dichroic concentrator (DM-OVSC-71), GaInP cell and TE module VI was characterized using the experimental setup shown in Fig. 2a. The power output from the PV cell and TE module were measured separately initially and then they were connected in series and measured as one unit. Fig. 9 illustrates the I-V, P-V and P-R curves for the PV cell, TE module and the hybrid PV-TE system, respectively. The key performance data are also listed in Table 4. It can be seen that the power output of the hybrid PV-TE system is higher than that of the PV cell alone by 6.3% owning to the contribution from thermoelectric generator, demonstrating clearly the advantage of the hybrid system. It is to be noted that the extra power from thermoelectric generator was obtained from IR spectrum without any adverse reduction in the power output from

the PV cell due to appropriate design of dichroic concentrator. Furthermore, the total power output from the hybrid system is 5.3 times as large as the power output from the bare PV cell, providing experimental confirmation of using the dichroic mirrors for simultaneous spectral splitting and bean concentration.

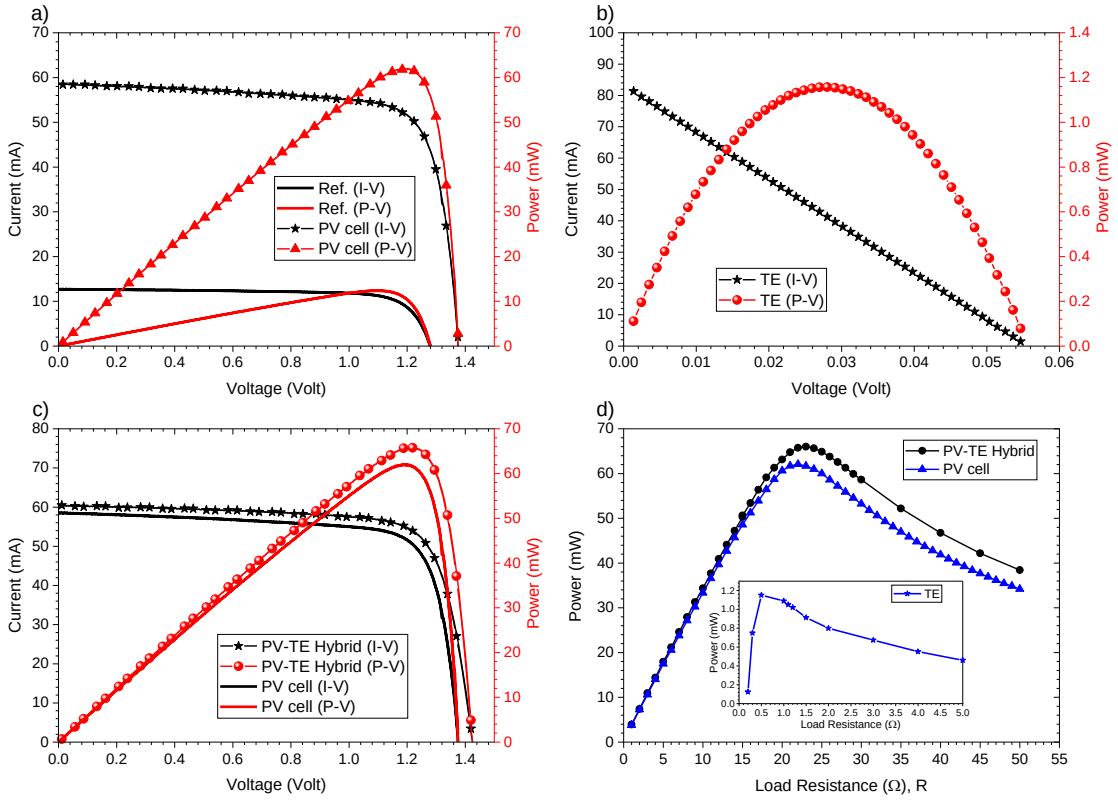

Fig. 9: The power output of hybrid PV-TE system. (a) I-V and P-V curves of the PV cell only, (b) I-V and P-V curves of TE module only, (c) I-V and P-V curves of PV-TE in series, compared with the PV cell only, (d) P-R curves of PV-TE in series, compared to PV cell only.

The results also show that the power output from TE module is very small compared to the power output from the PV cell due to small temperature difference across the TE module. Since the power output of the TE module is proportional to the square of temperature difference across the TE module, it is anticipated that power output of TE module can be increased by increasing the light intensity. Consequently, the hybrid PV-TE system was tested under a higher concentration of 1.5 sun (1500W/m^2), which is the highest light intensity available in the solar simulator employed. The results of the tests are listed in Table 4, together with those under 1.0 sun for comparison. The I-V, P-V and P-R curves for the PV cell, TE module and the hybrid PV-TE system under 1.5 sun are available in Appendix-A (Fig. A-6).

Table 4: The electrical parameters of the PV, TE and the hybrid PV-TE system under 1.0 sun and 1.5 sun.

Incident light	System	V_{oc} (± 0.002 Volt)	I_{sc} (± 0.02 mA)	FF %	P_{max} (± 0.01 mW)	η (%)
Ref.	**Bare PV cell**	1.280	12.74	75.81	12.41	14.6
1.0 sun	**PV**	1.370	58.59	77.00	62.04	15.9
	TE	0.050	81.33	26.03	1.16	0.5
	PV-TE	1.430	60.52	76.48	65.96	**16.9**
1.5 sun	**PV**	1.380	89.54	78.23	96.75	16.2
	TE	0.060	94.73	25.06	1.50	0.5
	PV-TE	1.440	91.03	75.82	99.65	**17.3**

It can be seen that the power outputs of the PV cell, TE module and PV-TE system are significantly increased. The overall efficiency of the PV-TE system is increased from 16.9% at 1.0 sun to 17.3% at 1.5 sun. Although the power output of the TE module is increased, the degree of increase is less than that of the PV cell.

This indicates that the heat loss from the thermal absorber becomes significant with increasing light intensity. In order to achieve the maximum benefit of increased light intensity, it is crucial to design more effective thermal absorber that can minimize the heat loss.

It is interesting to note that the power output generated by the hybrid PV-TE system, where the PV cell and TE modules are connected in series, was slightly higher than the sum of the power outputs from the PV cell and TE module measured separately. Numerical simulation based on the I-V data of the PV cell and TE module obtained from this experiment confirms this observation. However, the exact mechanisms responsible for this difference are not fully understood. Further investigation is needed.

4. Conclusions

A concentrated PV-TE system was designed and constructed using the dichroic mirrors for both spectral splitting and beam concentration to improve the efficiency of solar energy conversion by additional harvesting the "unused energy" in infrared spectrum. The performance of this hybrid system was investigated under the standard one-sun testing condition. The results show that the total efficiency of the hybrid system is 16.9% compared to 15.9% of the same configuration except for the reflecting surfaces of the concentrator being aluminium mirror. An increase in the overall efficiency by 6.3% was achieved by thermoelectric harvesting of the light energy in infrared spectrum. Compared to the bare cell that generates 12.41 mW, the same cell in the concentrated system produces 62.04 mW, indicating the advantages of using concentrator, particularly beneficial to the high-cost solar cells such as GaAs and GaInP. The hybrid system was also tested under the increase intensity of 1.5 sun, resulting in a further increase in the efficiency to 17.3% due to light concentration.

The experimental results show that the power output of the PV cell using a dichroic concentrator is as high as using a high-quality specular aluminum concentrator. This is achieved in an appropriately designed system, involving proper spectral allocation, careful selection of dichroic mirror, PV cell and TE module, and optimal design of the optical and thermal components. The study of the dependence of the power output on the geometry of TE modules shows that the size of the TE module plays an important role in minimizing the heat loss from the thermal absorber. Furthermore, it is possible to further increase the power output from TE module by improved design of thermal absorber.

It was found that the power output of the hybrid system measured by connecting the PV cell and TE module in series is higher than the sum of the power outputs measured separately from the PV and TE, respectively under identical testing conditions. Numerical analysis confirms this finding but the mechanisms responsible for this increase remains to be understood. An enhanced understanding of this effect could lead to further improvement.

Acknowledgement

One of the authors (M.A) would like to thank Mutah University, the Hashemite Kingdom of Jordan for the financial support of his PhD study. The authors acknowledge the SPECIFIC innovation and knowledge centre at Swansea University for EQE measurements. We would like to thank ALANOD GmbH & Co. KG, Germany for supplying the aluminium reflector sheets which have been used in this work. The technical staff at Cardiff School of Engineering are acknowledged for assistance in constructing the concentrated hybrid system. The facilities for solar cell characterisation were established with the funding support by EPSRC under the projects EP/K029142/1, EPK022156/1. Professor Andrew Knox and Professor Tapas Mallick are acknowledged for inspirational discussion that led to the initial concept of simultaneous spectral splitting and beam concentration using dichroic mirror during a SUNTRAP project meeting funded by EPSRC (EPK022156/1).

References

[1] Anwar, S., *Handbook of research on solar energy systems and Technologies*. 2012: IGI Global.

[2] Narducci, D., et al., *Hybrid and fully thermoelectric solar harvesting*. Vol. 268. 2018: Springer.

[3] Shittu, S., et al., *Comprehensive study and optimization of concentrated photovoltaic-thermoelectric considering all contact resistances.* Energy Conversion and Management, 2020. **205**: p. 112422.

[4] Goldsmid, H.J., *Introduction to thermoelectricity*. Vol. 121. 2010: Springer.

[5] Pérez-Higueras, P. and E.F. Fernández, *High Concentrator Photovoltaics: Fundamentals, Engineering and Power Plants*. 2015: Springer International Publishing.

[6] Mohammadnia, A., et al., *Hybrid energy harvesting system to maximize power generation from solar energy.* Energy Conversion and Management, 2020. **205**: p. 112352.

[7] Hirst, L.C. and N.J. Ekins-Daukes, *Fundamental losses in solar cells.* Progress in Photovoltaics, 2011. **19**(3): p. 286-293.

[8] Mertens, K., *Photovoltaics: fundamentals, technology, and practice*. 2018: John Wiley & Sons.

[9] Tomar, V., B. Norton, and G.N. Tiwari, *A novel approach towards investigating the performance of different PVT configurations integrated on test cells: An experimental study.* Renewable Energy, 2019: p. 93-108.

[10] Sahin, A.Z., et al., *A review on the performance of photovoltaic/thermoelectric hybrid generators.* International Journal of Energy Research, 2020. **44**(5): p. 3365-3394.

[11] del Amo, A., et al., *An innovative urban energy system constituted by a photovoltaic/thermal hybrid solar installation: Design, simulation and monitoring.* Applied Energy, 2017. **186**: p. 140-151.

[12] Baranowski, L.L., G.J. Snyder, and E.S. Toberer, *Concentrated solar thermoelectric generators.* Energy & Environmental Science, 2012. **5**(10): p. 9055-9067.

[13] Sripadmanabhan Indira, S., et al., *A review on various configurations of hybrid concentrator photovoltaic and thermoelectric generator system.* Solar Energy, 2020. **201**: p. 122-148.

[14] Hashim, H., J.J. Bomphrey, and G. Min, *Model for geometry optimisation of thermoelectric devices in a hybrid PV/TE system.* Renewable Energy, 2016. **87**: p. 458-463.

[15] Min, G. and D.M. Rowe, *Optimisation of thermoelectric module geometry for 'waste heat' electric power generation.* Journal of Power Sources, 1992. **38**(3): p. 253-259.

[16] Russo, J.M., et al. *Analysis of dispersive spectrum splitting systems*. in *High and Low Concentrator Systems for Solar Energy Applications IX*. 2014. SPIE.

[17] Lan, D. and M.A. Green. *Pathways towards a 50% efficiency spectrum-splitting photovoltaic system: Application of built-in filters and generalization of concept*. in *12th International Photovoltaic Power Generation and Smart Energy Conference & Exhibition, SNEC 2018*. 2018. Elsevier Ltd.

[18] Yang, Z., et al., *Maximum efficiency and parametric optimum selection of a concentrated solar spectrum splitting photovoltaic cell-thermoelectric generator system.* Energy Conversion and Management, 2018. **174**: p. 65-71.

[19] Imenes, A.G. and D.R. Mills, *Spectral beam splitting technology for increased conversion efficiency in solar concentrating systems: A review.* International Solar Energy Society World Congress 2003, 2004. **84**(1-4): p. 19-69.

[20] Liang, H.X., et al., *Experimental investigation on spectral splitting of photovoltaic/thermal hybrid system with two-axis sun tracking based on SiO2/TiO2 interference thin film.* Energy Conversion and Management, 2019. **188**: p. 230-240.

[21] Sharaf, O.Z. and M.F. Orhan, *Concentrated photovoltaic thermal (CPVT) solar collector systems: Part I - Fundamentals, design considerations and current technologies.* 2015.

[22] Wingert, R., et al., *Spectral beam splitting retrofit for hybrid PV/T using existing parabolic trough power plants for enhanced power output.* Solar Energy, 2020. **202**: p. 1-9.

[23] Wang, G., et al., *Design and thermodynamic analysis of a novel solar CPV and thermal combined system utilizing spectral beam splitter.* Renewable Energy, 2020. **155**: p. 1091-1102.

[24] Liang, H., et al., *Experimental investigation on spectral splitting of photovoltaic/thermal hybrid system with two-axis sun tracking based on SiO2/TiO2 interference thin film.* Energy Conversion and Management, 2019. **188**: p. 230-240.

[25] Yazdanifard, F., M. Ameri, and R.A. Taylor, *Numerical modeling of a concentrated photovoltaic/thermal system which utilizes a PCM and nanofluid spectral splitting.* Energy Conversion and Management, 2020. **215**: p. 112927.

[26] An, W., et al., *Analysis of a temperature dependent optical window for nanofluid-based spectral splitting in PV/T power generation applications.* Energy Conversion and Management, 2017. **151**: p. 23-31.
[27] Al-Shohani, W.A.M., et al., *Experimental investigation of an optical water filter for Photovoltaic/Thermal conversion module.* Energy Conversion and Management, 2016. **111**: p. 431-442.
[28] Mojiri, A., et al., *Spectral beam splitting for efficient conversion of solar energy - A review.* Renewable and Sustainable Energy Reviews, 2013. **28**: p. 654-663.
[29] Mitchell, B., et al., *Four-junction spectral beam-splitting photovoltaic receiver with high optical efficiency.* Progress in Photovoltaics: Research and Applications, 2011. **19**(1): p. 61-72.
[30] Stanley, C., A. Mojiri, and G. Rosengarten, *Spectral light management for solar energy conversion systems.* Nanophotonics, 2016. **5**(1): p. 161-179.
[31] Zhang, D., et al., *Optical performance of dichroic spectrum-splitting filters.* Journal of Photonics for Energy, 2014. **4**(1): p. 043095.
[32] Sullivan, B.T. and J.A. Dobrowolski, *Implementation of a numerical needle method for thin-film design.* Applied Optics, 1996. **35**(28): p. 5484-5492.
[33] Sullivan, B.T., et al., *Manufacture of complex optical multilayer filters using an automated deposition system.* Vacuum, 1998. **51**(4): p. 647-654.
[34] Kandilli, C. and G. Külahlı, *Performance analysis of a concentrated solar energy for lighting-power generation combined system based on spectral beam splitting.* Renewable Energy, 2017. **101**: p. 713-727.
[35] Mojiri, A., et al., *A spectrally splitting photovoltaic-thermal hybrid receiver utilising direct absorption and wave interference light filtering.* Solar Energy Materials and Solar Cells, 2015. **139**: p. 71-80.
[36] Piarah, W.H., et al., *The characterization of a spectrum splitter of Techspec AOI 50.0mm square hot and cold mirrors using a halogen light for a photovoltaic-thermoelectric generator hybrid.* Energies, 2019. **12**(3).
[37] Imenes, A.G., et al., *A new strategy for improved spectral performance in solar power plants.* Solar Energy, 2006. **80**(10): p. 1263-1269.
[38] Kim, S., et al., *Development of thin-film solar cells using solar spectrum splitting technique.* Solar Energy Materials and Solar Cells, 2013. **119**: p. 214-218.
[39] Macleod, H.A., *Thin-film optical filters*. 2017: CRC press.
[40] Sheng, R., et al., *Four-Terminal Tandem Solar Cells Using CH3NH3PbBr3 by Spectrum Splitting.* Journal of Physical Chemistry Letters, 2015. **6**(19): p. 3931-3934.
[41] Green, M.A. and A. Ho-Baillie, *Forty three per cent composite split-spectrum concentrator solar cell efficiency.* Progress in Photovoltaics: Research and Applications, 2010. **18**(1): p. 42-47.
[42] Green, M.A., et al., *40% efficient sunlight to electricity conversion.* Progress in Photovoltaics, 2015. **23**(6): p. 685-691.
[43] Vincenzi, D., et al., *Concentrating PV system based on spectral separation of solar radiation.* Physica Status Solidi (A) Applications and Materials Science, 2009. **206**(2): p. 375-378.
[44] Wang, X., et al., *Lateral spectrum splitting concentrator photovoltaics: Direct measurement of component and submodule efficiency.* Progress in Photovoltaics: Research and Applications, 2012. **20**(2): p. 149-165.
[45] Stanley, C., et al., *Performance testing of a spectral beam splitting hybrid PVT solar receiver for linear concentrators.* Applied Energy, 2016. **168**: p. 303-313.
[46] Jiachen, W., S.B. Lee, and K. Lee, *Design of broadband multilayer dichroic coating for a high-efficiency solar energy harvesting system.* Applied Optics, 2015. **54**(15): p. 4805-4811.
[47] Johnson, D., *Quantum and thermal conversion of solar energy to useful work.* Document TP-252-2137, 1983.
[48] Ju, X., et al., *A review of the concentrated photovoltaic/thermal (CPVT) hybrid solar systems based on the spectral beam splitting technology.* Applied Energy, 2017. **187**: p. 534-563.
[49] Skjølstrup, E.J.H. and T. Søndergaard, *Design and optimization of spectral beamsplitter for hybrid thermoelectric-photovoltaic concentrated solar energy devices.* Solar Energy, 2016. **139**: p. 149-156.
[50] Sibin, K.P., et al., *Design and development of ITO/Ag/ITO spectral beam splitter coating for photovoltaic-thermoelectric hybrid systems.* Solar Energy, 2017. **141**: p. 118-126.
[51] Wang, G., et al., *Thermodynamic and optical analyses of a hybrid solar CPV/T system with high solar concentrating uniformity based on spectral beam splitting technology.* Energy, 2019. **166**: p. 256-266.

[52] Wang, G., et al., *Design and thermodynamic analysis of a novel solar CPV and thermal combined system utilizing spectral beam splitter.* Renewable Energy, 2020. **155**: p. 1091-1102.
[53] Al-Najideen, M., M. Al-Shidhani, and G. Min. *Optimum design of V-trough solar concentrator for photovoltaic applications*. in *15th International Conference on Concentrator Photovoltaic Systems, CPV 2019*. 2019. American Institute of Physics Inc.
[54] *Edmund Optics Ltd, Cold Mirror, #64-451*. 2016: USA.
[55] *GaAs and GaInP cells, Arima Photovoltaic & Optical Corporation*. 2017: Taiwan.
[56] *Direct Copper Bonded (DCB) Ceramic Substrates, Tianjin Century Electronics, China* 2017.
[57] *PNM400 (Matt Black), High Temperature Paint, RS 250-6976, Electrolube- HK Wentworth Group*. 2017: UK.
[58] *RS PRO Type K Thermocouple 1m Length, 1/0.2mm Diameter*. 2016: UK.
[59] *RS PRO Heat Sink Compound Plus Silicone Thermal Grease, 2.9W/m·Km RS 217-3835*. UK.
[60] *Alanod-Solar, MIRO-SUN® reflective 95, ALANOD GmbH & Co. KG, Germany*. 2017.
[61] *LCS-100 Series Small Area Solar Simulators*, N.C. Oriel Instruments, Editor. 2013, Newport Spectra-Physics Ltd.,: USA.
[62] *Metrohm Autolab B.V., Instruments for electrochemical research*. 2013: The Netherlands.
[63] *StellarNet, Inc., StellarNet Spectroscopy Instrumentation*, StellarNet, Editor. 2016, USA.
[64] *Kipp & Zonen B.V., CMP-10 Pyranometer* 2014: The Netherlands.
[65] Kazuz, R., *Hybrid solar thermo-electric systems for combined heat and power*. 2014, Cardiff University.
[66] *European Thermodynamics Ltd., Leicestershire, LE8 0RX, United Kingdom*. 2018.
[67] Min, G., *Thermoelectric Module Design Under a Given Thermal Input: Theory and Example.* Journal of Electronic Materials, 2013. **42**(7): p. 2239-2242.
[68] Min, G., *Principle of determining thermoelectric properties based onI–Vcurves.* Measurement Science and Technology, 2014. **25**(8): p. 085009.
[69] Rowe, D.M. and G. Min, *Design theory of thermoelectric modules for electrical power generation.* IEE Proceedings: Science, Measurement and Technology, 1996. **143**(6): p. 351-356.
[70] García-Cañadas, J. and G. Min, *Low Frequency Impedance Spectroscopy Analysis of Thermoelectric Modules.* Journal of Electronic Materials, 2014. **43**(6): p. 2411-2414.
[71] Good, P., et al., *Spectral reflectance, transmittance, and angular scattering of materials for solar concentrators.* Solar Energy Materials and Solar Cells, 2016. **144**: p. 509-522.
[72] Kostic, L.T., T.M. Pavlovic, and Z.T. Pavlovic, *Influence of reflectance from flat aluminum concentrators on energy efficiency of PV/Thermal collector.* Applied Energy, 2010. **87**(2): p. 410-416.
[73] Sharaf, O.Z. and M.F. Orhann, *Concentrated photovoltaic thermal (CPVT) solar collector systems: Part II - Implemented systems, performance assessment, and future directions.* Renewable and Sustainable Energy Reviews, 2015. **50**: p. 1566-1633.
[74] Shanks, K., S. Senthilarasu, and T.K. Mallick, *Optics for concentrating photovoltaics: Trends, limits and opportunities for materials and design.* Renewable and Sustainable Energy Reviews, 2016. **60**: p. 394-407.
[75] Jamali, H., *Investigation and review of mirrors reflectance in parabolic trough solar collectors (PTSCs).* Energy Reports, 2019. **5**: p. 145-158.

Appendix

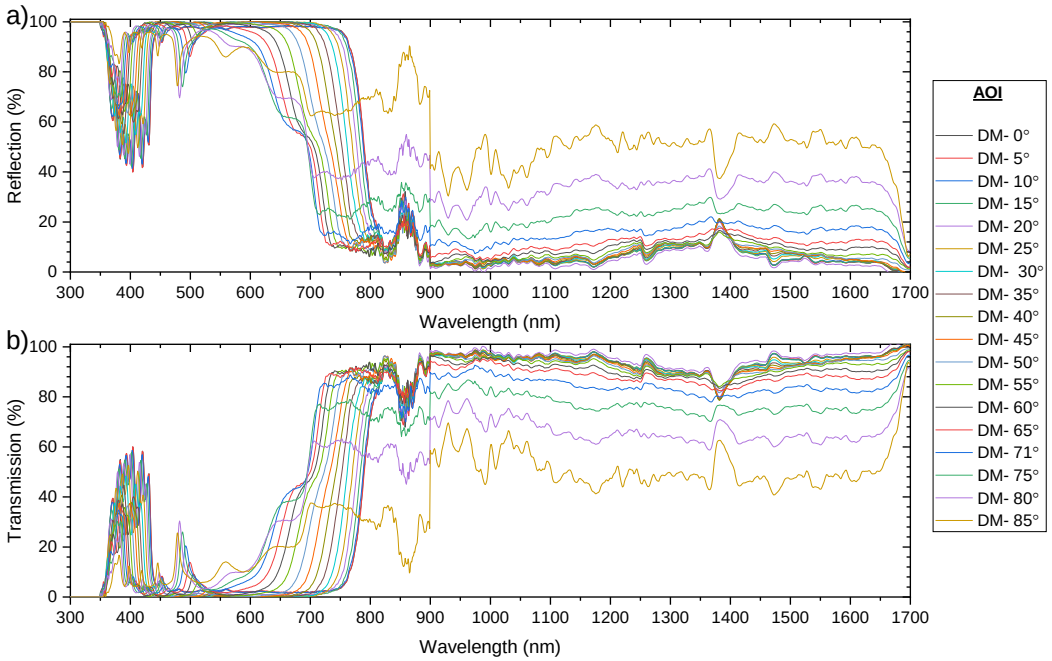

Fig. A-1: Spectral characteristics of the DM at different AOIs; a) the spectral reflectance; and b) spectral transmittance.

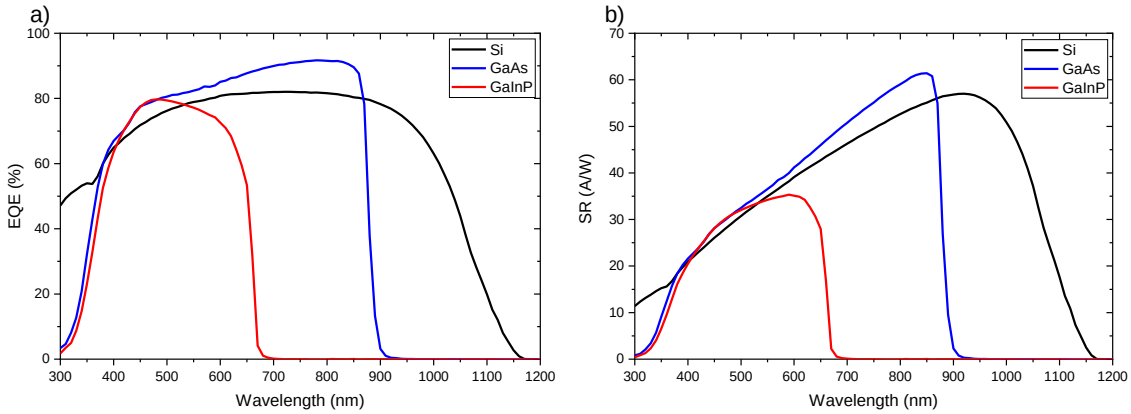

Fig. A-2: a) Experimental results of external quantum efficiency (EQE) for Si, GaAs and GaInP cells. b) Experimental results of the spectral response (SR) for Si, GaAs and GaInP cells.

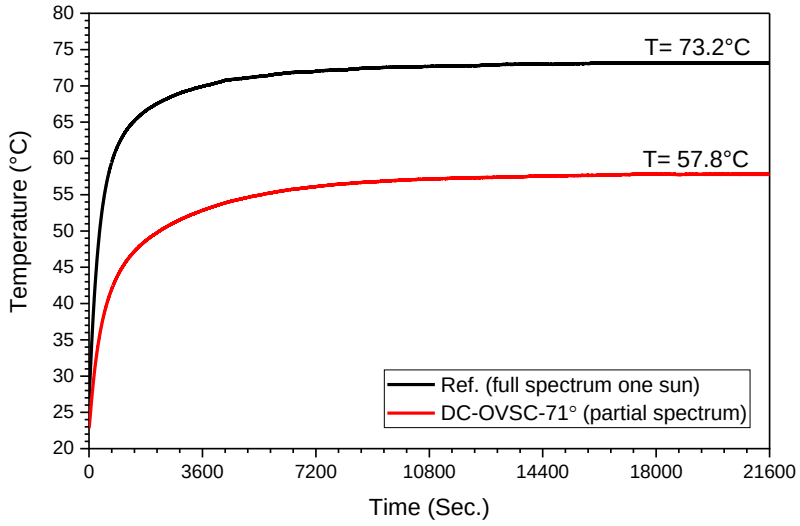

Fig. A-3: The heating profile of the thermal absorber of the PV-TE system (isolated, not connected to TE). The black curve shows the temperature increase of the absorber under full spectrum illumination while the red curve shows the temperature increase of the absorber under partial spectrum illumination using the dichroic mirrors.

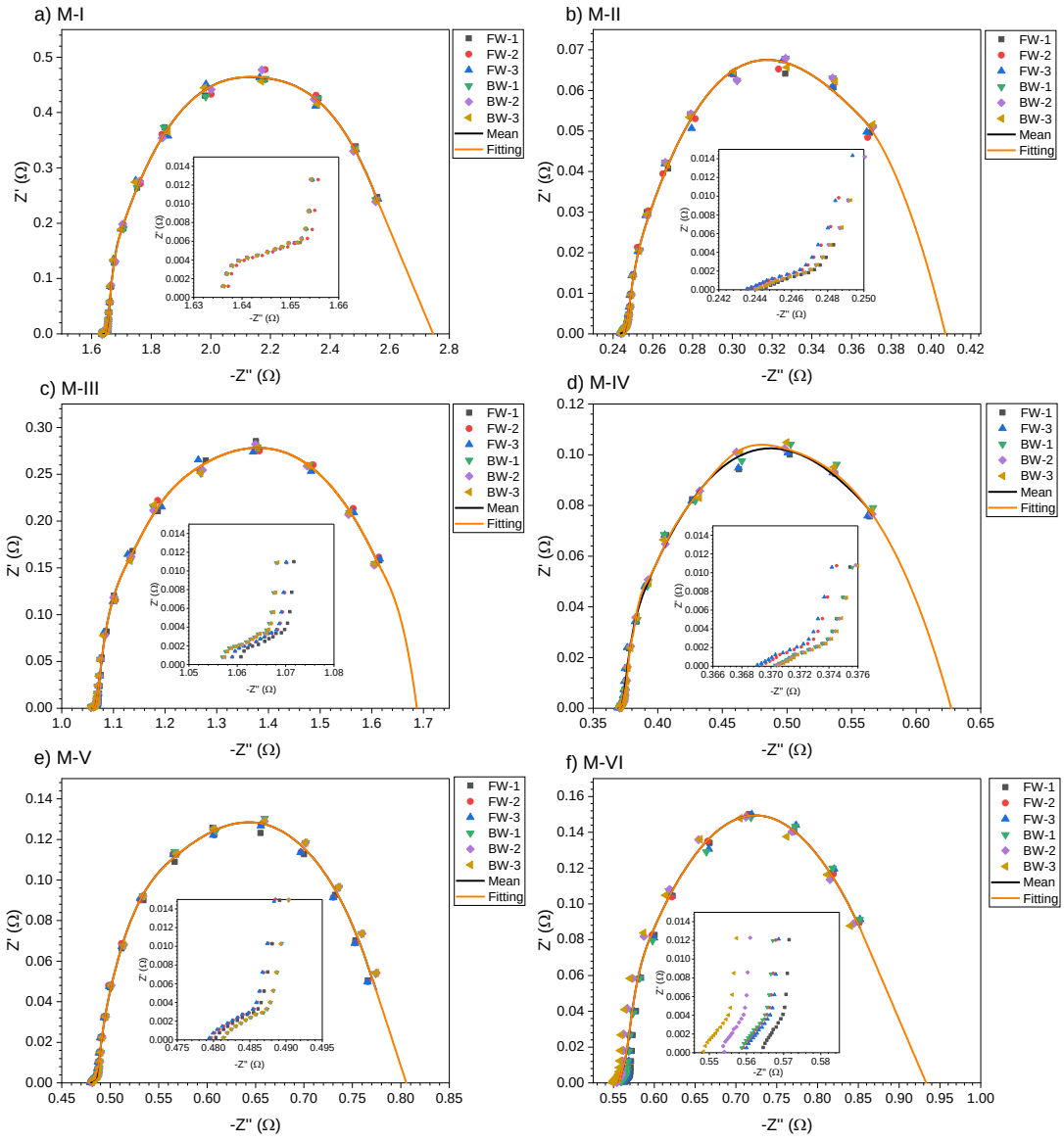

Fig. A-4: Nyquist plot (Impedance spectroscopy) of the TE modules.

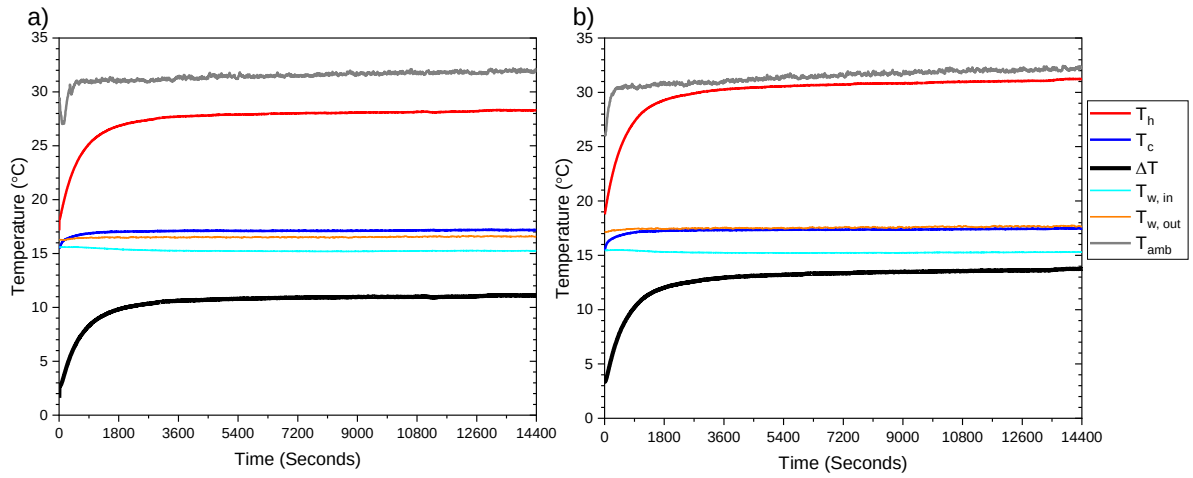

Fig. A-5: The temperatures across the TE module in the hybrid PV-TE system under a) one sun irradiance; and b) increased light irradiance of 1.5 sun. Th, Tc, ΔT are the temperatures of the hot, cold and the difference between them. $T_{w,in}$, $T_{w,out}$ and T_{amb} are the temperatures of the water inlet and outlet and the ambient.

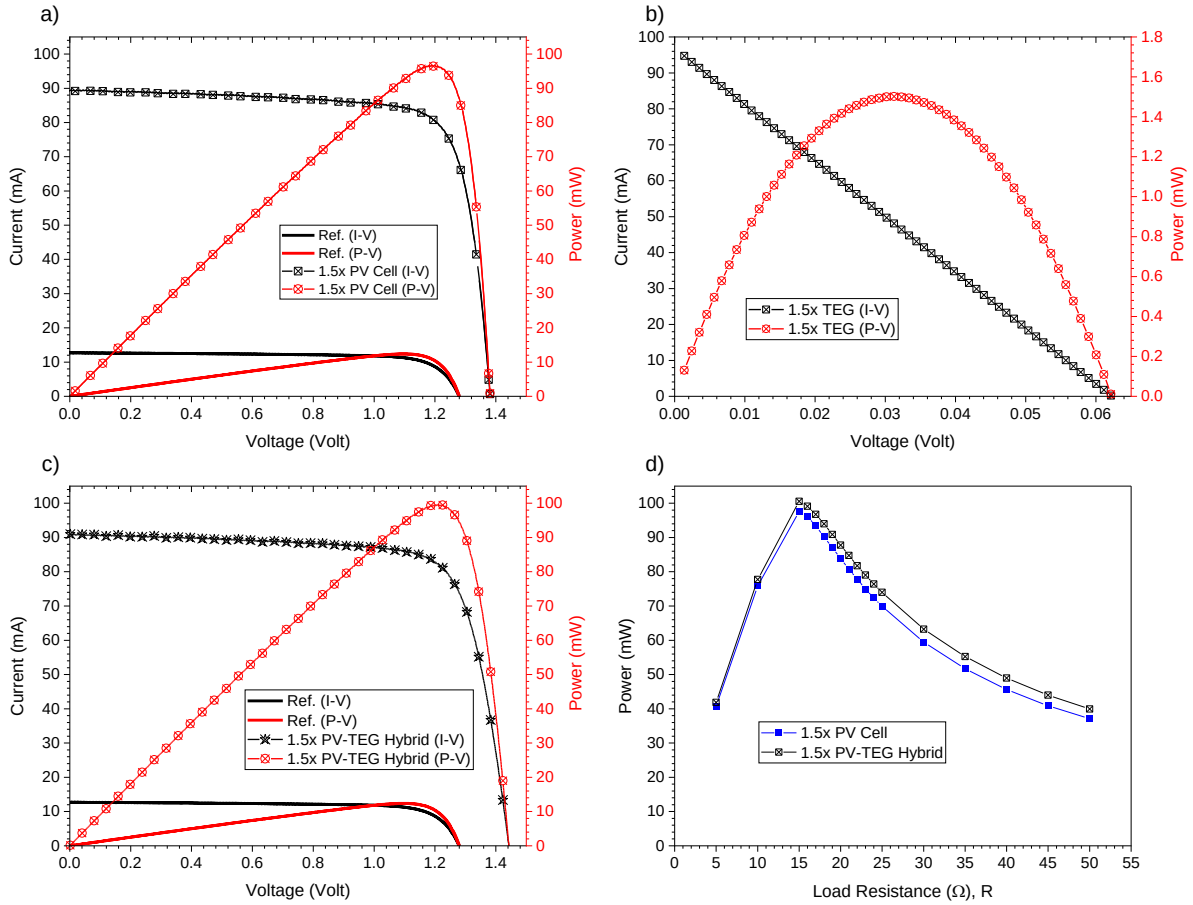

Fig. A-6: The power output of hybrid PV-TE system under increased light irradiance of 1.5 sun. (a) I-V and P-V curves of the PV cell only, (b) I-V and P-V curves of TE module only, (c) I-V and P-V curves of PV-TE in series, compared with the PV cell only, (d) P-R curves of PV-TE in series, compared to PV cell only.